# Section Sensitivity on Mechanical Properties in Pearlitic Spheroidal Graphite Iron Castings with Heavy Section

Satoshi Yamamoto
Daiwa Heavy Industry Co., Ltd, Hiroshima City, Japan

Haruki Itofuji
I2C Technology institute Co., Ltd, Ube City, Japan

Minoru Hatate
Kindai University, Higashihiroshima City, Japan

Sadato Hiratsuka
Iwate University, Morioka City, Japan



## ABSTRACT

The effects of section sensitivity on tensile, impact and fatigue properties in pearlitic spheroidal graphite iron (P-SGI) castings were investigated using sand-molded samples with a modulus from 1.25 to 5 cm. The most influential factor on the section sensitivity of tensile properties was found to be the microstructure of network-ferrite and pearlite precipitated along the prior austenite grain boundaries. This network-ferrite precipitated at modulus over 4.1 cm. For impact properties, the absorbed energy in the transition region tended to increase as the spacing of the pearlite layers became refined. These section sensitivity on tensile, impact and fatigue properties were improved by normalizing.

**Keywords:** section sensitivity, heavy section castings, spheroidal graphite cast iron, tensile property, impact property, fatigue property, normalizing, network ferrite

## INTRODUCTION

Pearlitic spheroidal graphite iron (P-SGI) is generally used as a high-strength material under a variety of conditions because it can be produced economically and exhibits excellent tensile properties. In addition, the use of these materials is expected to expand in the future, as they are expected to help realize a low-carbon society by replacing steel and reducing the wall thickness of products in response to recent global environmental issues. Therefore, the effects of graphite nodules and microstructure on the mechanical properties of spheroidal graphite iron castings with heavy sections are important issues to consider. Against this background, in recent years, spheroidal graphite cast iron for large castings has often been used to evaluate materials with a cast test sample or a sample cut from the heavy section of the product to assure the quality of the material. However, in heavy-section SGI, mechanical properties are reduced due to the lower solidification cooling rate caused by the product shape.[1] This section sensitivity is more pronounced for P-SGI than for ferrite-SGI, and although this is thought to be due to the conversion of pearlite to ferrite, the detailed cause is not clear.[2] In addition, the evaluation of fatigue strength is important for the application to members subjected to large loads, but there have been few reports on the section sensitivity of P-SGI to fatigue strength. In addition, in heavy section P-SGI, ferrite nucleates at the prior austenite grain boundary before pearlite is formed during eutectoid transformation.[3,4] This ferrite precipitates in a network along the prior austenite grain boundary (hereafter called “network-ferrite”) and is in direct contact with graphite, affecting its static mechanical properties.[5] In addition, there are concerns about the effects on dynamic mechanical properties, but there are no clear research reports.[4]

In this study, the effects of section sensitivity and network-ferrite on mechanical properties were investigated by melting a metal equivalent to FCD600 and using samples with different solidification cooling rates, assuming that the strength of the actual product is guaranteed. The effect of Ni addition was also investigated since materials contained Ni was expected as a countermeasure against section sensitivity on tensile properties.

## EXPERIMENTAL PROCEDURE

### MELTING OF MODULUS SAMPLES

The material grade of FCD600(JIS G 5502) was selected as P-SGI. Base molten irons were prepared using a 25ton high-frequency induction furnace. Pig iron and steel scrap were used as raw materials. Copper was selected as base alloy element to obtain P-SGI. Additionally, Ni was added as a sub element. The influence of Mn was also

surveyed because its unfavorable effects for heavy sections. Spheroidizing and inoculation were performed using the sandwich method. For Ni containing Mg-treated iron, post stream inoculation was conducted to prevent the formation of chunky graphite. Table 1 shows the chemical composition of the inoculants, the spheroidizer used and the amounts added. For the analysis of chemical composition, chilled test samples were taken from the same treated molten metal and analyzed using optical emission spectrometry (OES). The modulus samples were made of furan sand, and a common downgate was used so that they could be cast at the same time to ensure uniform experimental conditions. A schematic diagram of the casting design is shown in Fig. 1.The shape of the modulus samples was as shown in Fig. 2 in order to change the cooling rate in five stages. For the calculation of modulus, M1.25 to M3 were calculated using the flat plate formula (area c /2 in Figure 2, M4.1 and M5 were calculated using volume/surface area.[6] Feeder was provided for M1.25 to M3 as in the Y-type sample. The samples containing Ni were evaluated with M1.25 and M4.1 only.

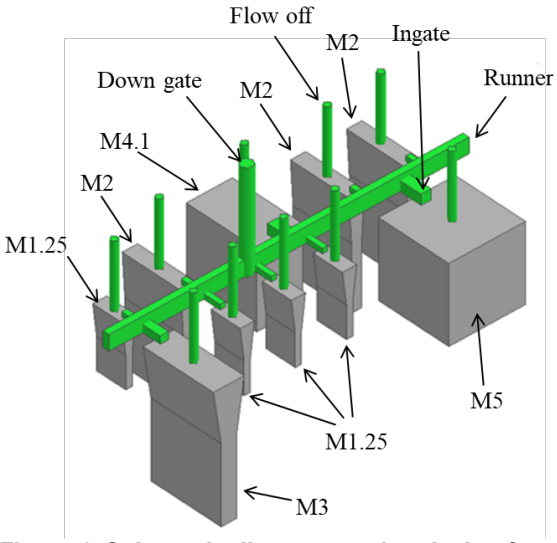


***Figure 1. Schematic diagram casting design for modulus samples.***

***Table 1. Chemical Composition of Inoculations and Spheroidizer Agent***

| Alloys | Chemical composition and additives, mass% | | | | | | | | Addition,wt% |
|---|---|---|---|---|---|---|---|---|---|
| | Si | Mg | Ca | Al | Ba | Zr | La | Fe | |
| Spheroidizer agent | 46.9 | 6.52 | 0.84 | 0.75 | - | - | 0.01 | Bal. | 1.00 |
| Primary inoculant | 48.9 | - | 0.46 | 1.03 | - | - | - | Bal. | 0.80 |
| Post inoculant | 74.4 | - | 2.26 | 1.24 | - | 1.67 | - | Bal. | 0.10 |

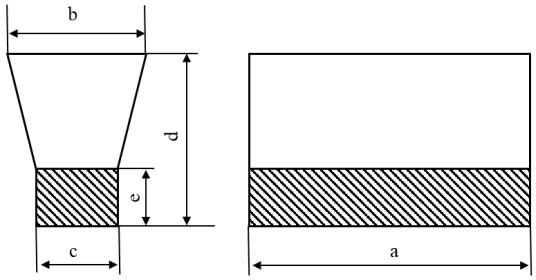


| Dimensions of each modulus (mm) | | | | | |
|---|---|---|---|---|---|
| M, cm | a | b | c | d | e |
| 1.25 | 125 | 55 | 25 | 250 | 125 |
| 2.00 | 250 | 80 | 40 | 420 | 250 |
| 3.00 | 300 | 120 | 60 | 500 | 300 |
| 4.10 | 300 | - | 180 | - | 300 |
| 5.00 | 300 | - | 300 | - | 300 |

***Figure 2. Dimensions of each modulus sample.***

## COOLING CURVE OF MODULUS SAMPLES

K-Type thermocouples were placed at the center of the wall thickness in each sample to measure the cooling curve. The solidification time was calculated using thermal analysis software (EPIC) and was defined as the time from the start of primary crystal reaction to the end of eutectic reaction. The average cooling rate from 825-775C (1517-1427F) just above the eutectoid transformation temperature was also calculated.

## HEAT TREATMENT OF SAMPLES

Normalized material was taken from the center of each modulus sample. The normalized samples were then cut into approximately 25 x 25 x 120 mm pieces, heated in a holding furnace at a rate of 80°C/144°F per hour, held at 880C (1616F) for 2 hours, and then air cooled. The samples containing Ni were the as-cast material.

## MICROSTRUCTURAL ANALYSIS

Microstructural analysis was performed by cutting at the grip of the tensile specimens, polishing the surface, and observing the specimen with an optical microscope at the magnification of 100x magnification for five views each. The graphite nodularity, nodule size, nodule count, and pearlite area percentage were calculated using image processing software. Graphite nodule smaller than 10 μm was eliminated from the image processing according to ISO-945. In the investigation of the pearlite structure, a scanning electron microscope (SEM) was used to draw a line perpendicular to the cementite in the pearlite, and the spacing between the ferrite and cementite layers that make up the pearlite microstructure at the intersection with that line was measured by the Linear Intercept Method. In addition, the fracture surface after the impact test was observed by SEM. The sample position observed was at the outer edge where tensile stress acts on the specimen at rupture to cause it to fracture. The fracture

surface after fatigue testing was also observed near the starting point of fracture using SEM.

### TENSILE TEST

Tensile tests were conducted at room temperature at a tensile speed of 1.0 mm/min using an Instron-type testing machine, with specimens taken from the center of each modulus sample, 8 mm in diameter at the parallel and 50 mm in length (gauge length is 40mm).

### IMPACT TEST

An instrumented Charpy impact testing machine with a capacity of 300 J was used for the impact test. The specimens were unnotched specimens of 10 × 10 × 55 mm, and load-displacement curves were measured. The impact transition temperature was calculated from the relation between temperature and impact absorption energy. Impact specimens were conditioned in a mixture of dry ice, liquid nitrogen, and organic solvents below room temperature and in heated oil above room temperature. For the impact test, the specimens were held at the target temperature for at least 15 minutes, after which the specimens were removed and tested within 5 seconds.

### FATIGUE TEST

Fatigue tests were conducted at room temperature using a rotating bending fatigue testing machine with specimens of 8 mm in diameter at the parallel section at a rotational speed of 3400 rpm. The number of cycles until the fatigue test was terminated was $1\times10$.[7]

## EXPERIMENTAL RESULTS

### CHEMICAL COMPOSITION AND COOLING CURVE OF MODULUS SAMPLES

Table 2 shows the results of the compositional analysis of each specimen (tensile test, impact test, fatigue test, Ni-0.5, Ni-1.5, Ni-2.0), with Mn ranging from 0.29% to 0.34% and no significant variation in the other chemical composition values. The Ni values for Ni-contained samples ranged from 0.48 to 2.08%. Figure 3 shows the measured cooling curves of the center of each modulus sample, solidification time, eutectoid transformation initiation temperature, and average cooling rate just above the eutectoid transformation, and Fig. 4 shows the relation between modulus and solidification time. The method of calculating modulus is different for specimens M1.25-3 and M4.1 or later used in this study due to differences in shape. However, a good correlation was observed between modulus and solidification time, with little influence from differences in shape. The solidification time increased with increasing modulus. The average cooling rate just above the eutectoid transformation decreased with increasing modulus, and this trend became more pronounced after M4.1.

***Table 2. Chemical Composition of Each Sample***

(mass%)

| Sample name | C | Si | Mn | P | S | Mg | Cu | Ni |
|---|---|---|---|---|---|---|---|---|
| Tensile test | 3.60 | 2.31 | 0.34 | 0.007 | 0.006 | 0.052 | 0.67 | 0.02 |
| Impact test | | | | | | | | |
| Fatigue test | 3.58 | 2.24 | 0.32 | 0.016 | 0.009 | 0.057 | 0.54 | 0.02 |
| Ni0.5 | 3.50 | 2.21 | 0.29 | 0.020 | 0.010 | 0.048 | 0.49 | 0.48 |
| Ni1.5 | 3.53 | 2.21 | 0.29 | 0.020 | 0.012 | 0.048 | 0.52 | 1.33 |
| Ni2.0 | 3.48 | 2.20 | 0.30 | 0.020 | 0.013 | 0.052 | 0.57 | 2.08 |

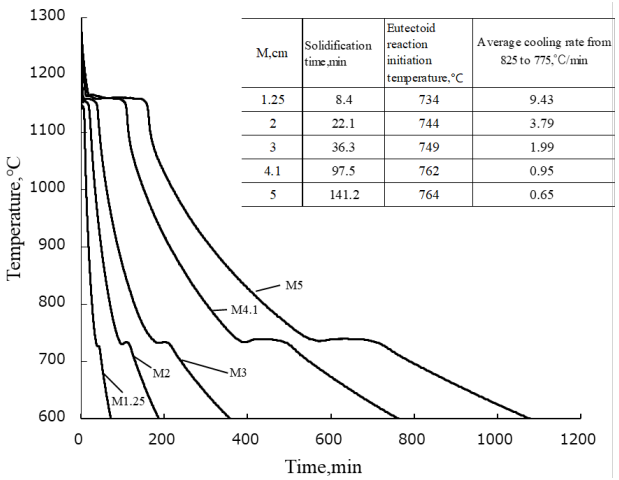


***Figure 3. Cooling curves at the center of modulus test blocks.***

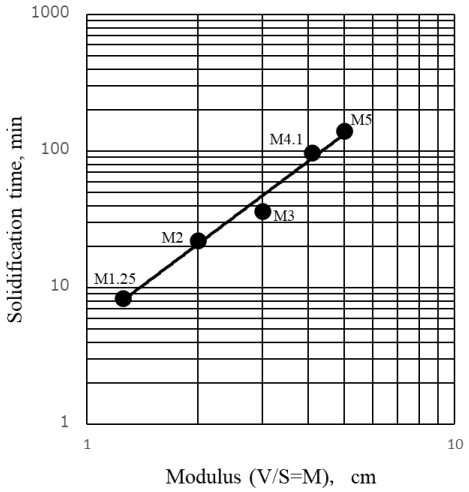


***Figure 4. Relation between modulus and solidification.***

In general, as the cooling rate decreases, the eutectoid transformation time increases and the ferrite area percentage increases due to eutectoid transformation in a stable system. Furthermore, the eutectoid transformation initiation temperature increases.[7]

The results of this study also suggest that the decrease in cooling rate affected the eutectoid transformation initiation temperature and eutectoid transformation time, and increased the amount of ferrite precipitated.

## RELATION BETWEEN MICROSTRUCTURE AND SOLIDIFICATION COOLING RATE

Figure 5 shows the microstructures of the as-cast and normalized samples taken from the center of each modulus sample, and Table 3 shows the results of their microstructural analysis. As modulus increased, the graphite nodularity decreased and the nodule size tended to increase, the nodule count decreased. The pearlite area percentage of the as-cast specimens varied significantly between M3 to M5, with a decrease to about 80% for M5. However, all samples had sound P-SGI castings with graphite nodularity and pearlite area percentage exceeding 80%. The precipitation of ferrite at the prior austenite grain boundary was limited to partial precipitation from M1.25 to M3, and network ferrite was observed to be more pronounced after M4.1, when the eutectoid transformation temperature increased to more than 760C (1400F) and the average cooling rate just above the eutectoid transformation was less than about 1°C (1.8°F)/min. In the model diagram of Johnson et al.[8] for the eutectoid transformation process of P-SGI, when eutectoid transformation starts with graphite existing in austenite above the eutectoid transformation temperature, ferrite is formed around the graphite and pearlite is formed from the prior austenite grain boundary. Subsequently, eutectoid transformation progresses and ferrite and pearlite grow to form a bullseye structure. However, the results of this study show that the eutectoid transformation of P-SGI is affected by the cooling rate. Therefore, a schematic diagram of the eutectoid transformation is shown in Fig. 6. In SGI, where the cooling rate is small, the graphite is surrounded by the austenite phase during solidification, and solidification proceeds by carbon diffusion through this solid phase or by grain boundary diffusion of carbon at the austenite grain boundaries,[9,10] Subsequently, as the temperature decreases, the carbon content of austenite decreases to the eutectoid concentration.[11] However, as Johnson et al. showed, in P-SGI with a large cooling rate, such as M1.25, ferrite forms around graphite, but carbon diffusion does not occur in time at the prior austenite grain boundary far from graphite, ferrite nucleation is difficult. On the other hand, in heavy section P-SGI with a small cooling rate such as M4.1, there is enough time for carbon to grain boundary diffusion, so the carbon concentration decreases at the prior austenite grain boundary in direct contact with graphite, and ferrite is formed at the prior austenite grain boundary. Then, as the temperature decreases, pearlite precipitates as the temperature decreases, forming the matrix structure with network ferrite characteristic of heavy section P-SGI. In all normalized samples, the network-ferrite disappeared and a slight ferrite was not observed in all specimens, resulting in a full pearlitic matrix structure. The graphite microstructure showed almost no change by normalizing and was almost the same as that of the as-cast.

***Table 3. Results of Microstructural Observation of Each Specimen***

| | M,cm | 1.25 | 3 | 5 |
|---|---|---|---|---|
| Graphite nodularity, % | Tensile test specimens | 88.6 | 85.6 | 81.6 |
| | Impact test specimens | | | |
| | Fatigue test specimens | 90.0 | 89.8 | 88.6 |
| Nodule size, μm | Tensile test specimens | 37.8 | 53.0 | 62.3 |
| | Impact test specimens | | | |
| | Fatigue test specimens | 40.6 | 47.4 | 51.9 |
| Nodules, count／$mm^2$ | Tensile test specimens | 109.0 | 53.0 | 40.0 |
| | Impact test specimens | | | |
| | Fatigue test specimens | 98.8 | 63.5 | 45.6 |
| Pearlite area percentage, % | Tensile test specimens | 93.8 | 92.0 | 83.9 |
| | Impact test specimens | | | |
| | Fatigue test specimens | 94.1 | 93.0 | 83.4 |

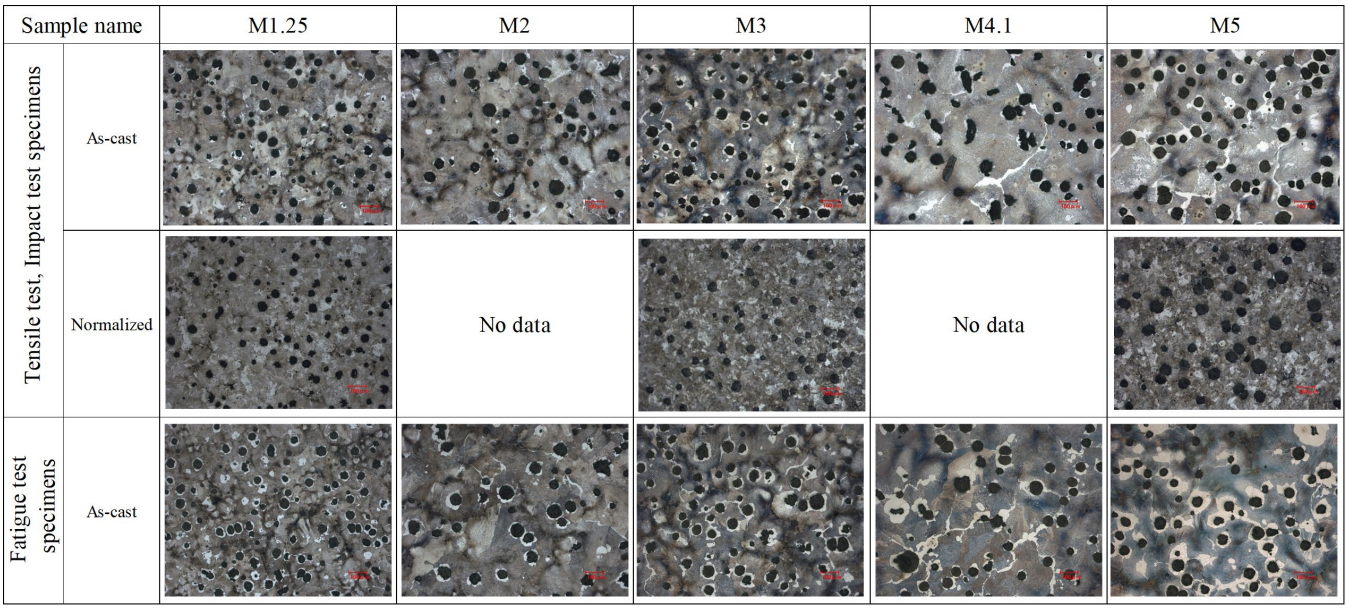


***Figure 5. Microstructures of as-cast and normalized samples (Nital etched).***

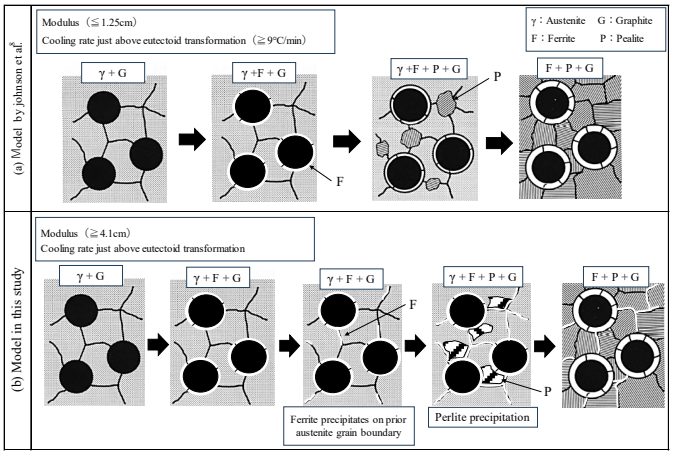


***Figure 6. Schematic diagram of eutectic transformation.[8]***

## SECTION SENSITIVITY OF TENSILE PROPERTIES

### TENSILE STRENGTH AND 0.2% PROOF STRESS

Figure 7 shows the relation between the tensile properties and modulus of the as-cast and normalized specimens. The tensile strength and 0.2% proof stress of the as-cast specimens decreased with increasing modulus. The reduction in tensile strength ranged from about 800 to 500 MPa, and the section sensitivity was greater than the 0.2% proof stress. Section sensitivity of tensile strength was more pronounced after M4.1. The reason for this is that the network-ferrite precipitates after M4.1 and serves as a crack propagation path for fracture, and the tensile strength depends on the strength of the network-ferrite.[5] On the other hand, the tensile strength of the normalized specimens increased for all specimens, and furthermore, no section sensitivity at 0.2% proof stress was observed in normalized specimens from M1.25 to M5. The decrease in tensile strength of M4.1 and M5 in the normalized specimen was less than that in the as-cast specimen. In other words, the tensile strength and 0.2% proof stress of section sensitivity are strongly affected by the matrix structure. Figure 8 shows the relation between the pearlite correlation spacing and tensile strength of the pearlite structure comprising P-SGI. The pearlite layer spacing of the as-cast material increased with increasing modulus, and the increase in pearlite layer spacing resulted in a decrease in tensile strength. However, the densification of pearlite layer spacing by normalizing significantly improved the tensile strength. Therefore, to clarify the relation between pearlite layer spacing and tensile strength, additional samples in Table 4, in which network-ferrite was not precipitated, were examined. In addition, the samples contained Mn did not affect the amount of network ferrite precipitated. The relation between tensile strength and pearlite layer spacing for all samples is shown in Fig. 9. The results show that the following approximate relation between tensile strength and pearlite-layer spacing for M1.25 to M3 is valid.

$$\sigma_B = 459.5 + 92.29 \times S^{-1} \qquad \textbf{Eqn. 1}^{12}$$

In this formula, $\sigma_B$ is the tensile strength (MPa) and S is the pearlite layer spacing (μm). Therefore, the section sensitivity of the tensile strength and 0.2% proof stress of as-cast material is strongly influenced by the synergistic effects of pearlite layer spacing expansion and network-ferrite formation.

***Table 4. Chemical Composition of Samples with Changing Mn***

(mass%)

| Sample name | C | Si | Mn | P | S | Mg | Cu |
|---|---|---|---|---|---|---|---|
| Mn0.1 | 3.50 | 2.18 | 0.12 | 0.009 | 0.007 | 0.051 | 0.65 |
| Mn0.3 | 3.57 | 2.27 | 0.32 | 0.018 | 0.009 | 0.054 | 0.65 |
| Mn0.6 | 3.59 | 2.22 | 0.54 | 0.011 | 0.010 | 0.046 | 0.72 |

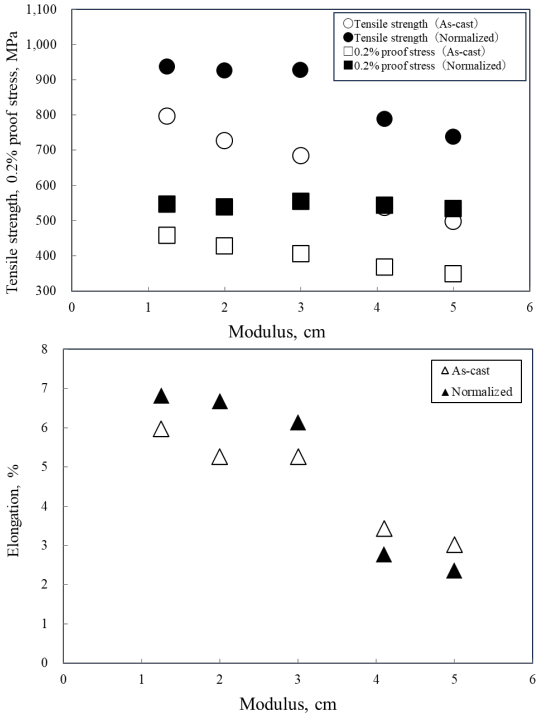


***Figure 7. Relation between static mechanical properties and modulus of as-cast and normalized specimens.***

### ELONGATION

The elongation of the as-cast material showed a decreasing trend despite the increase in ferrite area percentage as modulus increased. In other words, network-ferrite, which precipitates due to the decrease in solidification cooling rate, does not effectively improve elongation. On the other hand, the elongation of the normalized material was almost the same as that of the as-cast material, despite the pearlite formation of the matrix structure.

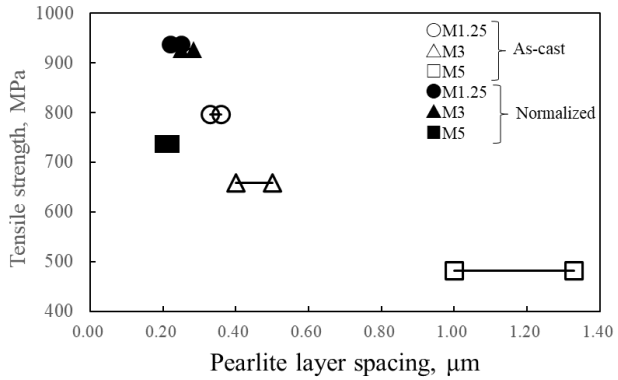


***Figure 8. Relation between pearlite layer spacing and tensile strength.***

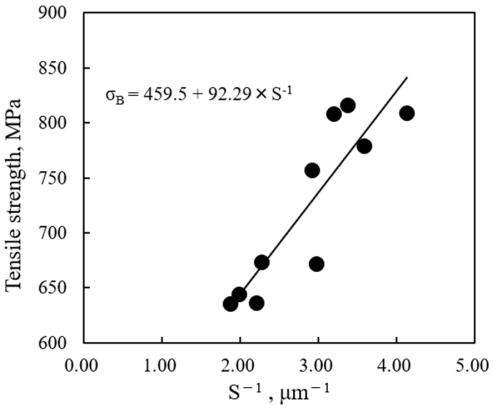


***Figure 9. Relation between spacing of pearlite layers and tensile strength of specimens.***

## SECTION SENSITIVITY OF IMPACT PROPERTIES

## EFFECT OF MICROSTRUCTURE ON IMPACT PROPERTIES

Figure 10 shows the impact transition curves for as-cast and normalized materials, as well as the transition temperatures. The impact transition curve of the as-cast material shows a transition from the ductile region to the brittle region as the temperature decreases.

The impact transition curve of the normalized material shifts to the lower temperature side than the as-cast material. In both the as-cast and normalized materials, the absorbed energy in the transition and ductile regions decreased with increasing modulus, indicating a section sensitivity. There is little difference in the absorbed energies in the ductile and brittle regions between the as-cast and normalized materials. However, the absorbed energy in the transition region of the normalized material is significantly higher. Therefore, the load-displacement curves of the impact fracture characteristics of the as-cast and normalized materials at room temperature in the transition region are shown in Fig. 11, and the fracture surface of the impact fracture at room temperature is shown in Fig. 12. This area occupied by the load-displacement curve represents the energy required for impact failure, and is classified as crack initiation energy (hereinafter called "Ei") up to the maximum load point and crack propagation energy (hereinafter called "Ep") thereafter.[13] Figure 11 shows that Ei dominates the impact fracture properties of the as-cast and normalized materials. In other words, ferrite precipitation generally increases Ep, but Ep is low in P-SGI, suggesting that network-ferrite has little effect on impact fracture properties. For fracture surfaces impact-fractured at room temperature, in the as-cast material M1.25, graphite nucleated dimples fracture surfaces were observed. However, M3 and M5 had more cleavage fracture surfaces and a stronger tendency toward brittle fracture. On the other hand, in the case of the normalized materials, graphite is less exposed and the cracks fracture across the pearlite phase. Furthermore, the fracture surface is a quasi-cleavage fracture, indicating that the fracture morphology is different from that of the as-cast material. In other words, the impact fracture of the normalized material in the transition region is affected by the matrix structure, and the densification of the pearlite structure due to normalizing is considered to have increased the Ei, contributing to the increase in absorbed energy.

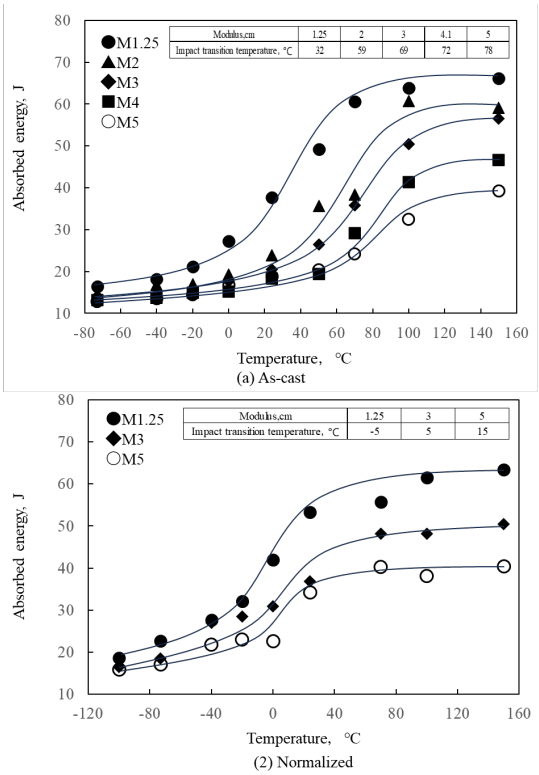


***Figure 10. Impact transition curves for as-cast and normalized specimens.***

Figure 13 shows the relation between absorbed energy and pearlite layer spacing at room temperature. Similar to tensile strength, absorbed energy tends to decrease with increasing pearlite layer spacing. The absorbed energies of M3 and M5 are comparable, and pearlite layer spacing above 0.40 μm is accompanied by a significant decrease in Ei. Therefore, the increase in the absorbed energy in the transition region in the normalized material is considered to be due to the densification of the pearlite structure.

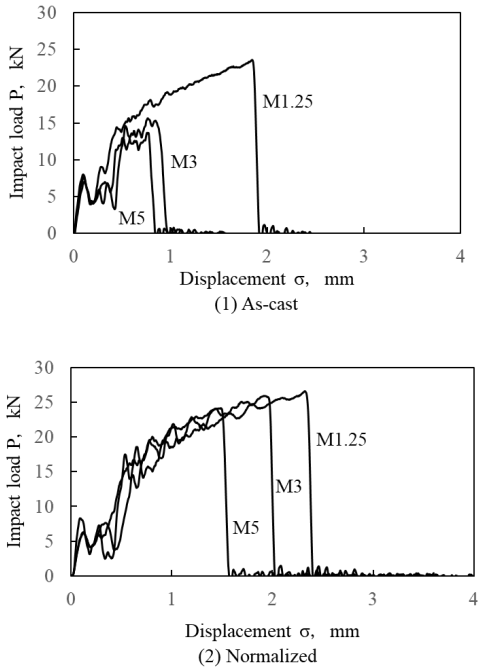


***Figure 11. Impact load-displacement curves obtained from instrumented impact test at room temperature.***

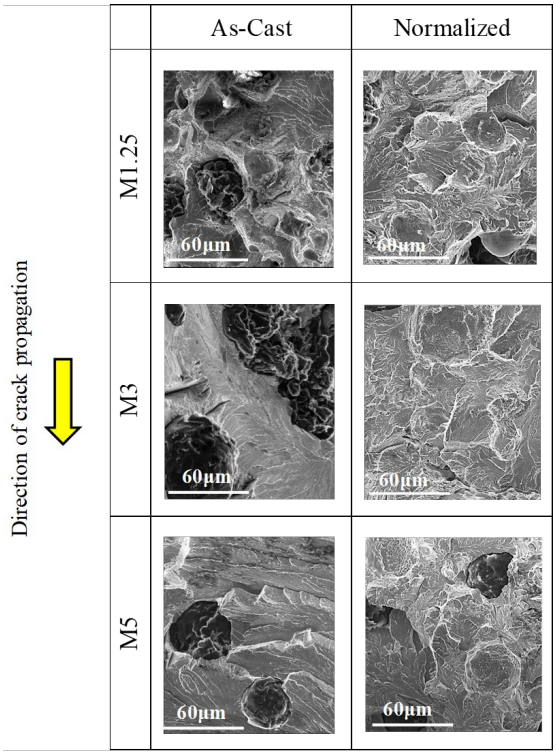


***Figure 12. SEM observation of impact fracture surfaces of as-cast and normalized specimens.***

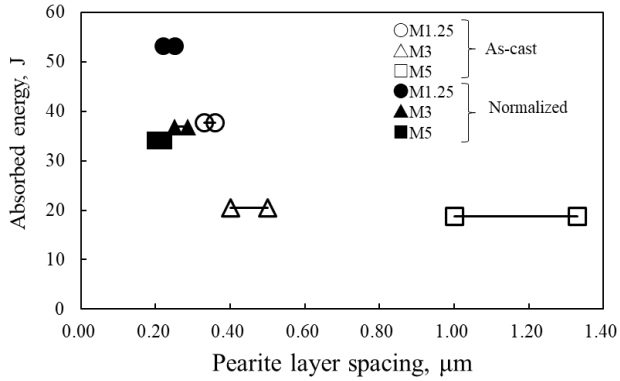


***Figure 13. Relation between pearlite layer spacing and absorbed energy.***

## EFFECT OF GRAPHITE ON IMPACT PROPERTIES

From graph (2) in Fig. 10, data shows that the difference in absorbed energy between the as-cast and normalized materials of M1.25 to M5 tends to increase from room temperature to the ductile region, reaching a maximum in the ductile region. Although the normalizing increased the absorbed energy in the transition region, no similar change was observed in the ductile region. Since the matrix structures of the normalized materials have nearly the same matrix structure due to heat treatment, the influence of the graphite structure is more pronounced in the region above room temperature. In general, the effect of graphite structure on P-SGI is that the transition behavior shifts to lower temperatures as the nodule size decreases, and furthermore, in the ductile region, there is a difference in absorbed energy depending on the nodule size. It is also known that a decrease in graphite nodularity increases the impact transition temperature.[14] The graphite nodularity of the normalized material with M1.25 to M5 ranged from 84.0 to 88.1%, and the effect of the graphite nodularity was considered to be slight, but the nodule size of the normalized material increased significantly with increasing modulus, ranging from 31.6 to 54.7 μm. Therefore, the reason why the difference in absorbed energy expands as modulus increases is that the fracture in the transition region and ductile region at temperatures higher than room temperature in P-SGI tends to cause microscopic ductile fracture when the nodule count increase,[15] and the displacement increases with plastic deformation. The graphite also acts as a crack propagation stop when a microcrack passes through, and the effect is enhanced by the increase in the nodule count. Therefore, the section sensitivity that occurs at temperatures higher than room temperature in the normalized material is considered to be caused by an increase in ductile fracture tendency of the microstructure due to an increase in nodule count and a decrease in the synergistic effect of graphite in stopping crack propagation.

## SECTION SENSITIVITY OF FATIGUE PROPERTIES

The S-N curves of the as-cast and normalized materials are shown in Fig. 14. The tensile strength and fatigue limit ratio (fatigue limit/tensile strength) are also shown in the figure. For both as-cast and normalized materials, section sensitivity was observed in the low-cycle side of the S-N curve and in the fatigue limit at $10^7$ cycles. Furthermore, the slope of the S-N curve of the normalized material became smaller, and the fatigue limit also increased compared to that of the as-cast material, transfer toward to the longer fatigue life.

In general, the following relation is recognized between tensile strength and fatigue limit of steel materials. Where: $\sigma_w$ is the fatigue limit of the steel and $\sigma_B$ is the tensile strength.

$$\sigma_W = 0.5\sigma_B \qquad \textbf{Eqn. 2}$$

However, the values of σw/σB for as-cast and normalized materials are 0.35-0.43 and 0.28-0.32, respectively, indicating that the fatigue limit of P-SGI castings with heavy section cannot be determined from the tensile strength because the values are lower than those in Eqn. 2. In addition, the tendency of the fatigue limit ratio to increase with increasing modulus in the as-cast material is considered to be due to the fact that the section sensitivity of the tensile strength is greater than the fatigue limit. Furthermore, the reduction in the fatigue limit of the as-cast materials was 21 MPa for M1.25 to M3 and 39 MPa for M3 to M5, which is remarkable after M3. On the other hand, the reduction in the fatigue limit of the normalized materials was limited to 39 MPa for M1.25 to M5, which was not as great as that of the as-cast materials. Figure 15 shows SEM observations of the crack initiation region of as-cast and normalized specimens that failed under fatigue loading of 300 MPa, and Fig. 16 shows the relation between the pearlite layer spacing and the fatigue limit. Fatigue fracture of all specimens started from the surface of the specimen where the maximum bending stress was applied, and many of the fractures were observed to start from defects or graphite in the vicinity of the surface. This means that the defects and graphite were dominant in determining the fatigue strength. However, in the case of M5, which is as-cast materials, there were also specimens in which near-surface defects and graphite, which are considered to be the most harmful from the viewpoint of fracture mechanics, were not observed. As for the relation between fatigue limit and pearlite layer spacing, the densification of pearlite layer spacing by normalizing significantly improved the fatigue limit of M5. However, the section sensitivity of the fatigue properties of the normalized material was not eliminated. In general, it has been noted that fatigue fracture of heavy section SGI may be initiated by microdefects or degenerated graphite.[17] The cast defects are often formed at cell boundaries, and the larger the eutectic cell, the larger the cast defect.[18] In other words, in SGI, the larger the graphite nodule size, the larger the eutectic cells, and the larger the cast defects tend to be. Murakami et al. proposed a simple Equation 3 to predict the fatigue limit of materials with small surface defects or cracks.[19]

$$\sigma w = \alpha \times (Hv+120) / (\sqrt{area})^{1/6} \qquad \textbf{Eqn. 3}$$

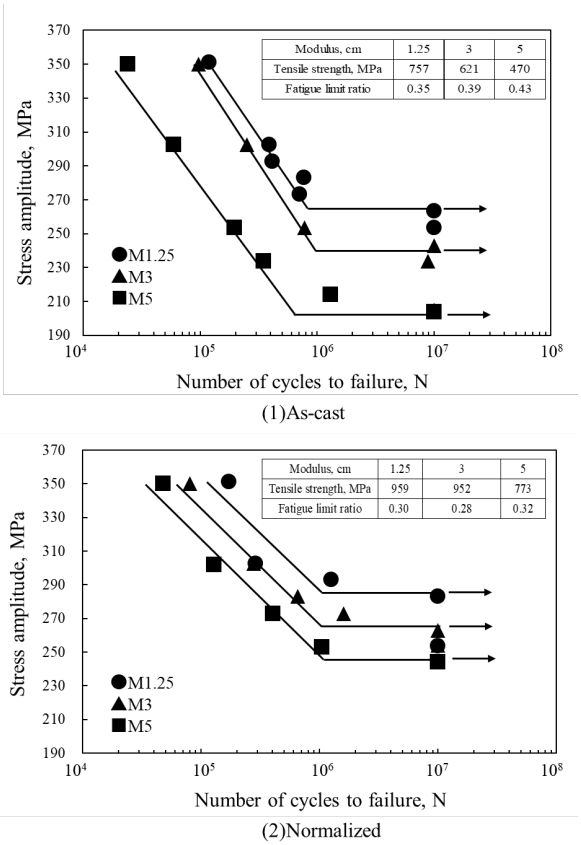


***Figure 14. S-N curves of as-cast and normalized materials.***

Where: σw (MPa) is the fatigue limit, α is the coefficient of defect location, Hv is the Vickers hardness(kgf/mm$^2$), √area (μm) is a geometric parameter, and the defect or crack is the square root of the area projected onto a plane perpendicular to the direction of maximum tensile force. From this equation, it can be seen that the fatigue limit is determined by the size of the defects and cracks and the hardness of the matrix structure. Therefore, the defect size and Vickers hardness of the as-cast material were measured, and the estimated fatigue limit was calculated. The results are shown in Table 5. The Vickers hardness test was conducted with a test load of 10 kg. The Vickers hardness of the as-cast material decreased with increasing modulus, and the defect dimensions increased. On the other hand, the Vickers hardness of M1.25 and M3 of normalized material were almost equal to 294 and 297 HV, respectively. In addition, M5 showed a marked increase compared to the as-cast material, although it decreased to 273 HV. This is thought to be due to the densification of pearlite layer spacing caused by the normalized. The defect dimensions were similar to those of the as-cast material, since the application of normalizing did not

affect the cast defects. The estimated fatigue limit was approximated by a value approximately 15% lower than the measured value.

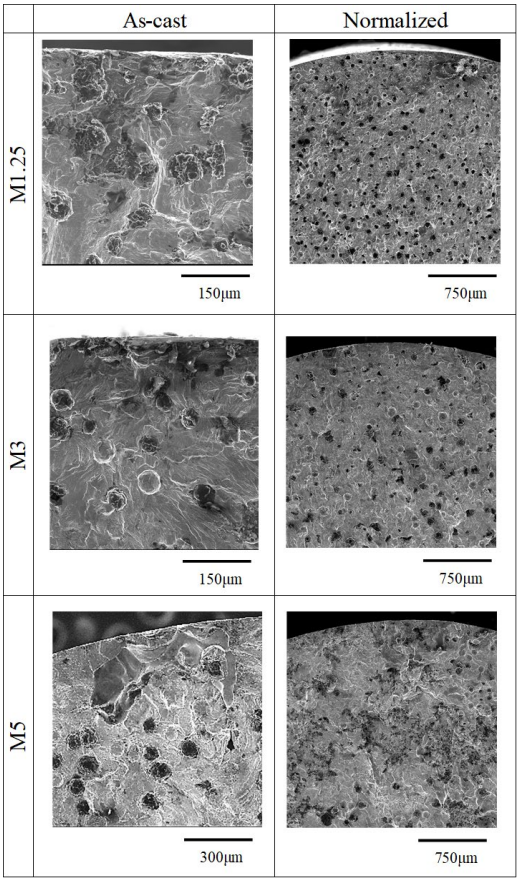


***Figure 15. SEM observation of crack initiation zone in fracture surfaces of specimens fractured at applied stress of 300MPa.***

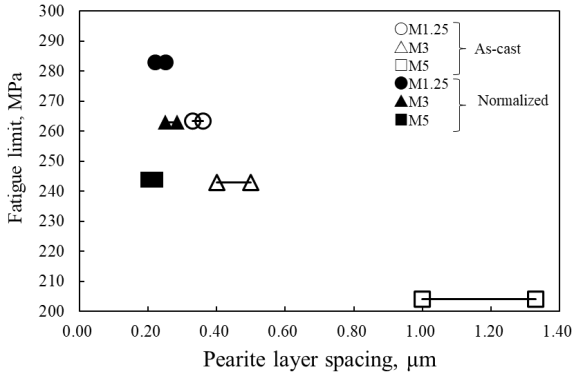


***Figure 16. Relation between pearlite layer spacing and fatigue limit.***

In other words, Equation (3) is valid for this material, and the cause of the lower fatigue limit is the increase in defect size and the decrease in hardness. Since hardness is considered to be affected by the pearlite layer spacing in normalizing, the section sensitivity with respect to fatigue properties is considered to be due to the increase in defects and graphite specific to heavy section P-SGI and the increase in crack growth rate of fatigue cracks due to the increase in pearlite layer spacing, resulting in a lower fatigue limit. Furthermore, the precipitation of network ferrite, which has lower fatigue strength than pearlite, is thought to contribute to the higher crack growth rate.

***Table 5. Vickers Hardness, Defect Dimensions & Fatigue Limit of As-Cast Specimens***

| | Vickers hardness, Hv | √area, μm | Fatigue limit estimated by √area, $\sigma_w$, MPa |
|---|---|---|---|
| M1.25 | 242 | 116.6 | 234 |
| M3 | 222 | 129.9 | 217 |
| M5 | 195 | 278.4 | 176 |

## EFFECT OF NI ON TENSILE PROPERTIES OF P-SGI

## MICROSTRUCTURE OF NI-ADDED SAMPLE

Figure 16 shows the microstructure of each Ni contained sample. Table 6 shows the results of microstructural analysis. The graphite morphology of both M1.25 and M4.1 increased in the nodule count and decreased in nodule size due to the effect of post inoculation compared to the as-cast material used in the fatigue tests. the matrix structure, ferrite structure was observed around graphite in M1.25 Ni0.5, but full pearlite structure was observed in Ni1.5 and Ni2.0. The pearlite area percentage also tended to increase with increasing Ni content. On the other hand, in M4.1, the pearlite area percentage tended to increase with Ni addition, and the network-ferrite precipitation tended to decrease, but the pearlite area percentage decreased compared to that in M1.25.

***Table 6. Results of Microstructural Analysis of Each Specimen***

| | M,cm | Ni0.5 | Ni1.5 | Ni2.0 |
|---|---|---|---|---|
| Graphite nodularity, % | 1.25 | 92.5 | 93.9 | 88.8 |
| | 4.1 | 89.9 | 91.9 | 93.4 |
| Nodule size, μm | 1.25 | 24.9 | 24.5 | 22.9 |
| | 4.1 | 46.0 | 45.1 | 45.7 |
| Nodules, count／$mm^2$ | 1.25 | 204.2 | 197.4 | 175.8 |
| | 4.1 | 87.6 | 74.1 | 75.7 |
| Pearlite area percentage, % | 1.25 | 87.7 | 90.9 | 93.0 |
| | 4.1 | 85.6 | 92.7 | 88.8 |

## TENSILE PROPERTIES OF NI-ADDED SAMPLES

Figure 17 shows the relations between tensile strength, 0.2% proof stress and the amount of Ni contained, and Fig. 18 shows the relations between elongation and the amount of Ni contained. The tensile properties of the specimens without Ni were those used in the fatigue tests. The tensile strength of M1.25 increased significantly with increasing Ni. On the other hand, the tensile strength of

M4.1 increased with Ni, but the increasing trend slowed down in the range of 0.5% to 2.0%. However, the 0.2% proof stress increased with increasing Ni in both M1.25 and M4.1, showing a good correlation between Ni amount and proof stress. Elongation showed a maximum value at 0.5% Ni and a tendency to decrease at higher Ni amounts. However, despite the increase in tensile strength due to the addition of Ni, the elongation values were similar to those of the samples without.

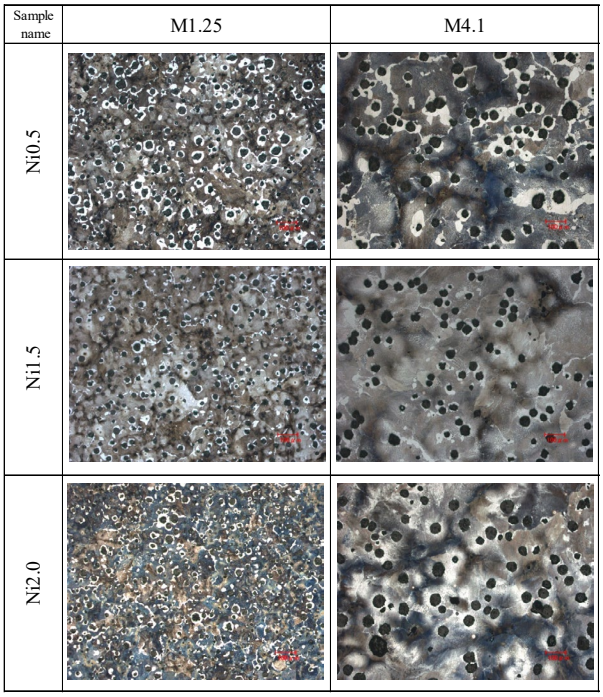


***Figure 16. Microstructures of Ni-added samples (Nital etched).***

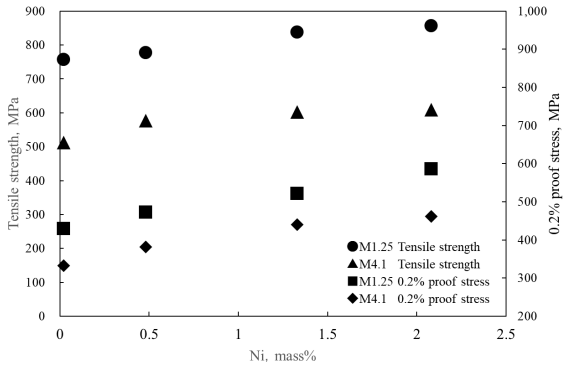


***Figure 17. Relation between tensile strength, 0.2% proof stress and Ni addtion.***

## SEM ANALYSIS RESULTS OF NI-ADDED SAMPLES

Figure 19 shows the SEM observation results of the Ni contained sample. There was little difference in pearlite layer spacing between the Ni0.0 and Ni contained samples of M1.25. In the M4.1, pearlitic layer spacing, the addition of Ni added to refine the pearlite layer spacing, but there was little difference between the samples with 0.5 to 2.0% Ni. In other words, the tensile strength of M1.25 is considered to have increased by strengthening ferrite in the lamellar structure of the pearlitic structure due to the addition of Ni. In M4.1, the addition of Ni tended to refine the spacing of pearlite layers and suppressed the precipitation of network-ferrite.

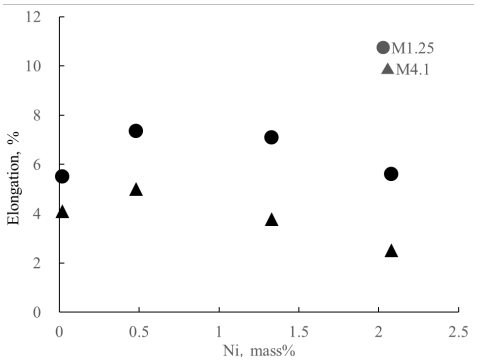


***Figure 18. Relation between tensile elongation and Ni addtion.***

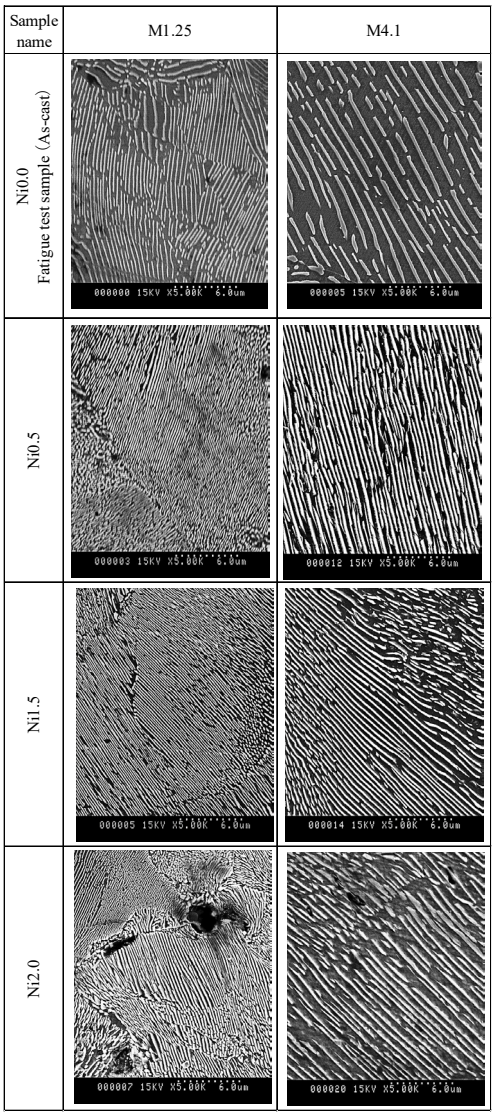


***Figure 19. Observation interlayer of pearlite in as-cast and Ni-added samples (×5000).***

However, network-ferrite precipitation was not eliminated. In other words, the addition of Ni in M4.1 strengthens ferrite in pearlite as in M1.25 and also strengthens network-ferrite, which is thought to have increased the tensile strength. Therefore, to ensure the substantive strength of large pearlitic SGI castings with heavy section, the combined addition of Cu and Ni in the range of 0.5% and 0.5% to 1.5%, respectively, is effective.

## CONCLUSIONS

### SECTION SENSITIVITY OF TENSILE PROPERTIES

1) The section sensitivity of as-cast material is more pronounced in tensile strength than in 0.2% proof stress by the synergistic effects of increasing pearlite layer spacing and network ferrite formation.
2) The section sensitivity of the tensile properties of the normalized material reduced compared to the as-cast material.

### SECTION SENSITIVITY OF IMPACT PROPERTIES

1) The section sensitivity of as-cast materials is clearly indicated by the absorbed energy of the transition and ductile regions. The main factor, the transition region is pearlite layer spacing. In the ductile region, the graphite grain size has an effect.
2) In the case of normalized materials, the absorption energy in the transition region is improved by refining the pearlite layer spacing.

### SECTION SENSITIVITY OF FATIGUE PROPERTIES

1) The section sensitivity of the as-cast material is more pronounced on the low-cycle side and at the fatigue limit. In addition, M5 is affected by increased pearlite layer spacing and network ferrite formation in addition to defect size.
2) In the case of the normalized material, the fatigue limit increases due to densification of the iron matrix structure, but the section sensitivity remains due to the effect of defect dimensions.

### HEAT TREATMENT IN HEAVY SECTION P-SGI

1) Normalizing is an effective heat treatment for improving the tensile properties of pearlitic spheroidal graphite iron castings with heavy section.

### EFFECT OF NI ON TENSILE PROPERTIES OF PEARLITIC SPHEROIDAL GRAPHITE IRON CASTINGS WITH HEAVY SECTION

1) At M1.25, tensile strength increases significantly with increasing Ni addition. However, the tendency of M4.1 is the same as M1.25 but slows down.
2) Even at M4.1, where the cooling rate is small, the addition of about 0.5% Cu and 0.5 to 2.0% Ni ensures a tensile strength of about 600 MPa.

## REFERENCES


1. N. Tsutsumi, T. Nagase, “Studies on the Mass-Effect of Spheroidal Graphite Iron,” *IMONO,* Vol. 42, pp. 37-49 (1970).
2. J.R. Davis, “Cast Iron ASM Specialty Handbook,” *ASM International,* pp. 70 (1996).
3. B.V. Kovacs, “Pearlite Stabilization In Cast Irons,”*AFS Transaction,* Vol. 89, pp.79-96 (1981).
4. S.I. Karsay, “Ductile Iron Production I,” Q I T-Fer et Titane Inc., pp. 188 (1992).
5. S. Yamamoto, Y. Fujikawa, S. Mashiba, H. Itofuji, M. Hatate, S. Hiratsuka, “Formation Mechanism of Network Ferrite in Heavy-Walled Pearlitic Spheroidal Graphite Iron Castings and Static Mechanical Properties,” *J.JFS,* pp. 474-481 (2023).
6. M. Matsuda, H. Nagasawa, T. Ono, H, Kimata, “A Method for Estimation of Solidification Time in Relation to Casting Shape,” *IMONO,* Vol. 61, pp. 314-319 (1989).
7. T. Kobayashi, “Influence of Cooling Rate on Ferrite Formation in Cast Iron,” *IMONO,* Vol. 47, pp. 555-561 (1975).
8. W.C. Johnson and B.V. Kovacs, “The Effect of Additives on the Eutectoid Transformation of Ductile Iron,” *Metallurgical Trans*. A, Vol. 9A, pp. 219-229 (1978).
9. H. Morrogh, “The Solidification of Metals,*” Iron and Steel Inst.,* pp. 238 (1968).
10. G. Jolley, “The Solidification of Metals,” *Iron and Steel Inst*., pp. 242 (1968).
11. T. Kanno, “Solidification Characteristics of Cast Steel and Cast Iron,” *J.JFS, Vol.* 85, pp. 522-533 (2013).
12. A.R. Marder, B.L. Bramfitt, “The Effect of Morphology on the Strength of Pearlite,” *Metallurgical Trans. A*, Vol. 7A, pp. 372 (1976).
13. T, Kobayashi, “Impact Fracture Characteristics of Cast Iron,” *Tetsu-to-Hagané*, Vol. 12, pp. 1578-1591 (1973).
14. T. Shiota, S. Komatsu, “Influence of Graphite Nodule Diameter on Impact Test Characteristics of Spheroidal Graphite Cast Iron,” *Journal of The Society of Materials Science Japan,* Vol. 30, pp. 387-393 (1981).
15. T. Shiota, M. Hatate, S. Komatsu, T. Matsuoka, “Influence of Carbon Content on the Impact Characteristics of Spheroidal Graphite Cast Iron,” *IMONO,* Vol. 65, pp. 771-776 (1993).
16. S. Yamamoto, Y. Fujikawa, S. Mashiba, H. Itofuji, M. Hatate, S. Hiratsuka, “Effects of Solidification Cooling Rate and Heat Treatment on Impact Properties of Heavy-Walled Pearlitic Spheroidal Graphite Iron Castings,” *J.JFS*, pp. 482-488 (2023).

17. T. Borsato, P. Ferro, F. Berto and C. Carollo, “Fatigue strength improvement of heavy-section pearlitic ductile iron castings by in-mould inoculation treatment,” *International Journal of Fatigue*, Vol. 102, pp. 221-227 (2017).
18. Y. Sugiyama, K. Asami, H. Wakasa, “Fatigue Limit of Ductile Cast Iron and Its Evaluation Method,” *IMONO, Vol.* 66, pp. 666-671(1994).
19. Y. Murakami, M. Endo, “Effect of Hardness and Crack Geometry on $\Delta K_{th}$ of Small Cracks,” *zairyou*, Vol. 35, pp. 911-917 (1986).